THE ASTROPHYSICAL JOURNAL, 411:351–361, 1993 July 1

ON THE NATURE OF THE POLARIZATION OPPOSITION EFFECT EXHIBITED BY SATURN'S RINGS

MICHAEL I. MISHCHENKO
NASA Goddard Institute for Space Studies, Hughes STX Corporation, 2880 Broadway, New York, NY 10025
Received 1992 July 9; accepted 1992 December 31

ABSTRACT

Saturn's A and B rings exhibit two intriguing opposition phenomena, namely, the unusually narrow photometric and polarization opposition effects. Specifically, the intensity of the reflected light measured in the visible has a strong and very narrow peak centered at zero phase angle and superposed on a smooth photometric phase curve, while the reflected polarization, being zero at zero phase angle, becomes negative and almost reaches its maximum negative value at a small phase angle of several tenths of degree. The small angular width of both phenomena makes it difficult to explain them on the basis of the commonly used shadowing models. On the other hand, it is known from controlled laboratory experiments and theoretical studies that a strong and very narrow opposition peak in the reflected intensity can be produced by coherent backscattering of light from powder-like layers composed of small regolithic grains. Recently, Mishchenko and Dlugach assumed that macroscopic particles of Saturn's rings are covered with a layer of submicrometer-sized regolithic ice grains and demonstrated that coherent backscattering of sunlight from this layer can explain the unusually narrow photometric opposition effect observed for Saturn's A and B rings in the visible. In this paper, we use a rigorous *vector* theory of coherent backscattering, developed recently for very small (pointlike) scattering grains by Ozrin, to show that for subwavelength-sized regolithic particles, the photometric opposition effect is accompanied by a polarization opposition effect of the same angular width. The common origin of the two coherent opposition phenomena was also demonstrated in recent controlled laboratory experiments by van Albada, van der Mark, and Lagendijk, although different terminology was exploited. These results may be considered an evidence that the polarization opposition effect observed for Saturn's rings in the visible has the same origin as the photometric opposition effect and is due to coherent backscattering of light from the regolithic layer composed of the submicrometer-sized ice grains.

A remarkable opposition brightening similar to that for Saturn's rings has also been observed for some icy satellites and E-type asteroids. It is suggested that if the regolithic grains responsible for the observed opposition spikes are smaller that the wavelength, then the polarization opposition effect should also be observed for these objects at phase angles less than 1 degree.

Subject headings: minor planets — planets and satellites: individual (Saturn) — polarization — radiative transfer

1. INTRODUCTION

As is well-known, Saturn's A and B rings exhibit pronounced photometric (Müller 1983; Franklin & Cook 1965) and polarization (Lyot 1929; Dollfus 1979; Johnson et al. 1980) opposition effects at visible wavelengths. The photometric opposition effect is observed as a strong and very narrow intensity peak, which is centered at zero phase angle and is superposed on a smooth photometric phase curve (Fig. 1). The term "polarization opposition effect" means that polarization of the backscattered light, being zero at zero phase angle, becomes negative and almost reaches its maximum negative value at a very small phase angle of a few tenths of degree (Figs. 2 and 3). The angular semi-width of both the photometric and polarization opposition effects observed for Saturn's rings in the visible is nearly the same and is of about 0°.3.

Lyot (1929) and Johnson et al. (1980) have demonstrated that the measured polarization distinctly correlates in direction with the plane through the Sun, Saturn, and Earth rather than with the ring plane. This result convincingly shows that the polarization is the result of local scattering on the surface of individual macroscopic ring particles covered with frost rather than the result of multiple interparticle reflections. Also, since the angular width of the photometric and polarization opposition effects is the same, Johnson et al. concluded that both opposition phenomena are parts of the same physical process occurring within the frost layer covering individual ring bodies.

To explain the strong and unusually narrow photometric opposition effect exhibited by Saturn's rings, the classical shadowing model was widely used, according to which the observed opposition brightening is produced by mutual shadowing among macroscopic ring bodies (von Seeliger 1887; Bobrov 1961; Franklin & Cook 1965; Lumme, Irvine, & Esposito 1983). This model enables one to reproduce the observed angular width of the photometric opposition effect, but requires that Saturn's rings are many-particle-thick, and the volume density of the rings is very small. However, this requirement contradicts the results of dynamical modeling of Saturn's rings (e.g., Bridges, Hatzes, & Lin 1984; Wisdom & Tremaine 1988), according to which the rings are a monolayer of densely distributed bodies. This has led Cook, Franklin, & Palluconi (1973) to the conclusion that the observed opposition brightening is the result of local scattering on the surface of individual macroscopic ring bodies and may be produced by a mechanism like that observed by Oetking (1966) in his laboratory photometric measurements for high albedo powder-like

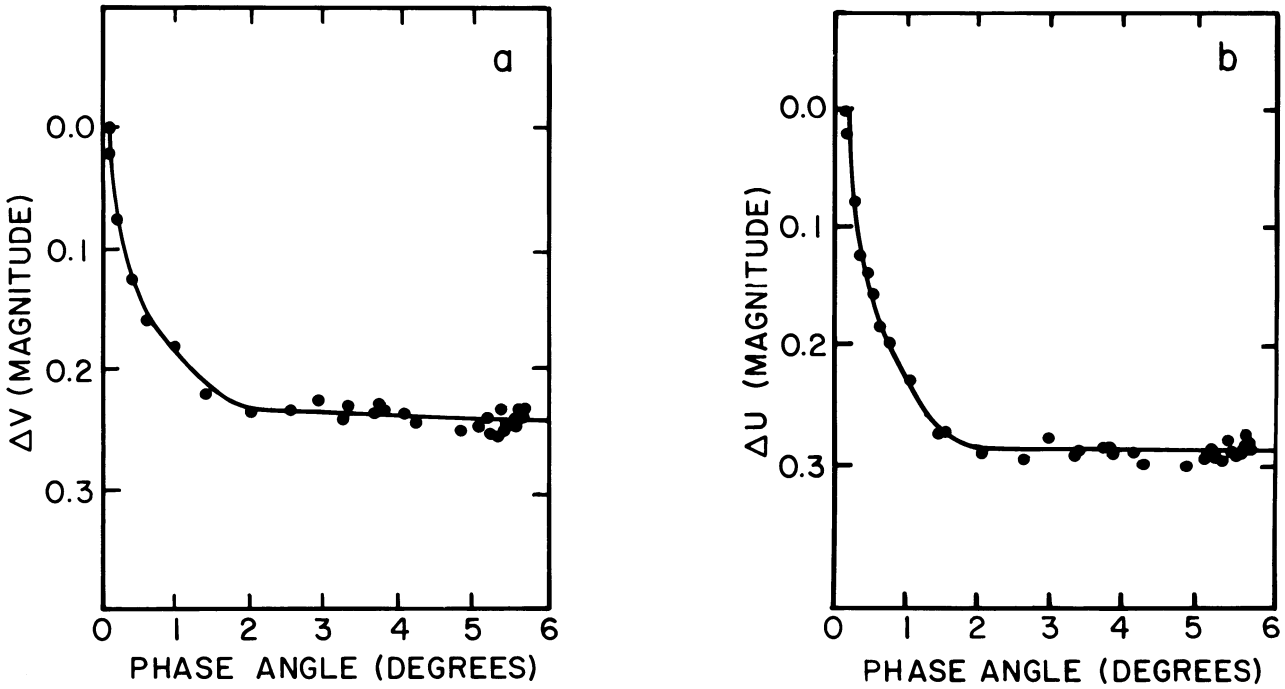

FIG. 1.—Visual (*a*) and blue (*b*) photometric opposition spikes for Saturn's A and B rings obtained after removal of a smooth component of the phase curve with a linear variation of 0.036 mag deg^{-1} (Franklin & Cook 1965).

surfaces. The discovery of similarly strong and narrow opposition spikes for many icy satellites (Franklin & Cook 1974; Brown & Cruikshank 1983; Goguen, Hammel, & Brown 1989; Domingue et al. 1991; Thompson & Lockwood 1992) and high albedo E-type asteroids (Harris et al. 1989; Lagerkvist et al. 1992) makes this conclusion rather well-grounded.

Opposition brightening and negative polarization at small phase angles have been observed for many atmosphereless solar system bodies (e.g., Bowell et al. 1989; Geake & Dollfus 1986; Dollfus et al. 1989). To interpret the photometric opposition effect, the same shadowing model was usually employed by assuming mutual shadowing among microscopic regolithic grains covering the surface of the bodies (e.g., Irvine 1966; Morozhenko & Yanovitskij 1971; Lumme & Bowell 1981; Hapke 1986). However, in the case of the ice-covered surface of ring bodies, it is not clear if the concept of a shadow is applicable to highly transparent icy regolithic grains. In addition, the small angular width of the photometric opposition effect exhibited by Saturn's A and B rings makes unlikely the explanation of this effect on the basis of the shadowing model since it requires unrealistically low volume density of the upper, optically active regolithic layer (e.g., Cook et al. 1973). Also, while for most of atmosphereless bodies the typical negative polariza-

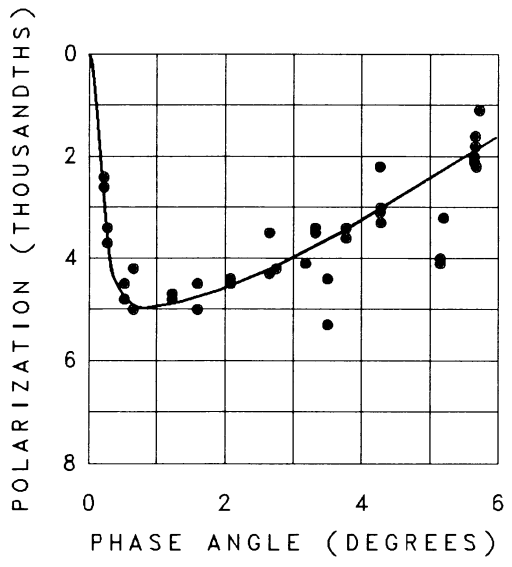

FIG. 2

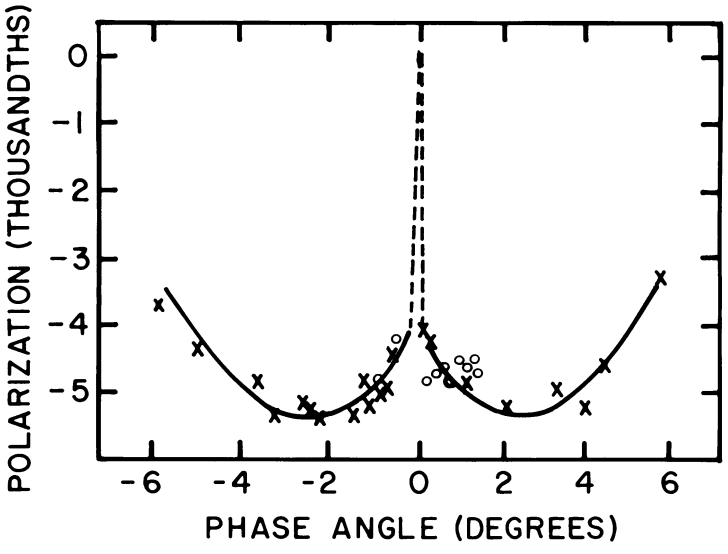

FIG. 3

FIG. 2.—Polarization opposition effect for the B ring of Saturn observed with a visual polarimeter (Lyot 1929)
FIG. 3.—Polarization opposition effect for Saturn's A and B rings observed with a standard *B* filter (Johnson et al. 1980)

tion branch has almost symmetric, nearly parabolic shape, in the case of Saturn's rings the negative part of the polarization phase curve is highly asymmetric, demonstrating a sharp rise of negative polarization at unusually small phase angles (Figs. 2 and 3). To explain the presence of the negative polarization branch on polarization phase curves observed for many atmosphereless bodies, the Wolff model or its modifications were often used (Wolff 1975, 1980; Kolokolova 1990; Wolff & Dollfus 1990), according to which the negative polarization branch is caused by shades and shadows affecting double-reflected rays. However, as was shown by Kolokolova, Mishchenko, & Wolff (1993), this model does not reproduce such a peculiar feature as the polarization opposition effect.

From controlled laboratory experiments and theoretical studies (e.g., Kuga & Ishimaru 1984; van der Mark, van Albada, & Lagendijk 1988; Wolf et al. 1988; Akkermans et al. 1988; Mishchenko 1991c), it is known that the so-called coherent backscattering of light from powder-like regolithic layers can produce a strong and narrow photometric opposition effect. Recently, Mishchenko & Dlugach (1992a) assumed that macroscopic particles of Saturn's rings are (partially) covered with a layer of small ice grains and demonstrated that both the width and amplitude of the observed photometric opposition effect are consistent with theoretical calculations of coherent backscattering for effective grain radii of several tenths of micrometer.

In explaining the polarization opposition effect, one should take into account that this phenomenon results from local scattering of sunlight on the surface of macroscopic ring bodies (Lyot 1929; Johnson et al. 1980), and its angular semi-width is equal to that of the photometric opposition effect, thus indicating that both phenomena are parts of the same physical process (Johnson et al. 1980). In this paper, we use a rigorous vector theory of coherent backscattering, developed recently for pointlike scatterers by Ozrin (1992b), to show that for subwavelength-sized regolithic grains, the coherent photometric opposition effect is accompanied by the coherent polarization opposition effect of the same angular width. The common interference nature of the two opposition phenomena has also been demonstrated in recent controlled laboratory experiments by van Albada, van der Mark, & Lagendijk (1988), although different terminology was exploited by these authors. These results enable us to suggest that the photometric and polarization opposition effects observed for Saturn's rings in the visible have the same origin and are due to coherent backscattering of sunlight from the regolithic layer composed of the submicrometer-sized ice grains.

2. THEORY AND LABORATORY MEASUREMENTS

To demonstrate the physical nature of coherent backscattering, let us first consider a surface element covered with a layer of small regolithic grains. Assume that this surface element is illuminated by sunlight which is incident in the direction given by the unit vector $\boldsymbol{n}_{\rm ill}$ and scattered toward the observer in the direction given by the unit vector $\boldsymbol{n}_{\rm obs}$ (Fig. 4). Let us consider a couple of conjugate light-scattering paths shown in Figure 4 by solid and dashed lines. These paths go through the same group of N regolithic grains, denoted in Figure 4 by their positions $\boldsymbol{r}_1, \ldots, \boldsymbol{r}_N$, but in the opposite directions. The waves scattered through the two conjugate paths will interfere, and the interference will be constructive or destructive depending on the phase difference between these light-scattering paths given by $k(\boldsymbol{n}_{\rm ill} + \boldsymbol{n}_{\rm obs})(\boldsymbol{r}_N - \boldsymbol{r}_1)$, where $k = 2\pi/\lambda$ is the wavenumber, and λ is the wavelength of light. If the observer is relatively far from exactly the backscattering direction given by $-\boldsymbol{n}_{\rm ill}$, the waves scattered by different groups of regolithic grains through the conjugate couples of light-scattering paths will interfere in different ways, and, due to the randomness of the medium, the average effect of interference will be zero. Thus, coherence will be lost, and the observer will measure some average, incoherent (diffuse) intensity, which is only weakly dependent on the phase angle α (the angle between the vectors $-\boldsymbol{n}_{\rm ill}$ and $\boldsymbol{n}_{\rm obs}$). However, at exactly the opposition ($\boldsymbol{n}_{\rm obs} = -\boldsymbol{n}_{\rm ill}$), the phase difference between the conjugate light-scattering paths is identically equal to zero for any group of regolithic grains, coherence is completely preserved, and the interference is always constructive, resulting in a coherent opposition peak.

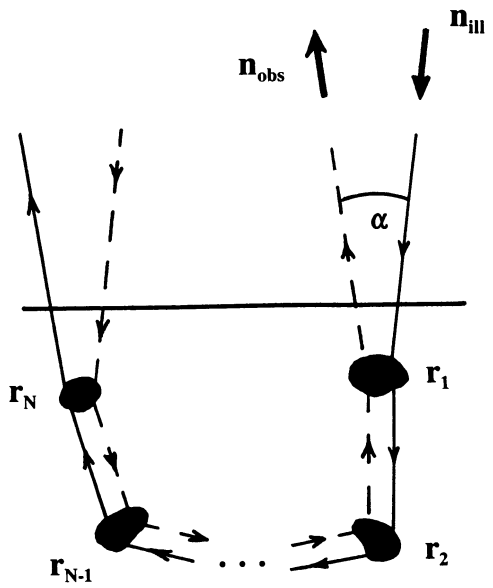

FIG. 4.—Schematic explanation of coherent backscattering

This somewhat simplified picture of coherent backscattering shows that the light reflected by the surface element consists of two parts. The first part comes from the incoherent multiple scattering by regolithic grains and is a slowly varying function of the phase angle. The second part comes from the coherent electromagnetic interaction of the grains and is nonzero only in the vicinity of the backscattering direction. Since the reflected light is, generally speaking, polarized, it must be specified by a four-component Stokes vector $\boldsymbol{I}$ having the Stokes parameters as its components as follows: $\boldsymbol{I} = \{I, Q, U, V\}$. Thus we have

$$\boldsymbol{I} = \boldsymbol{I}^D + \boldsymbol{I}^C , \tag{1}$$

where $\boldsymbol{I}^D$ is the diffuse, incoherent contribution and $\boldsymbol{I}^C$ is the coherent contribution.

At present, the interference nature of coherent backscattering is basically well understood, and the theory of multiple scattering of electromagnetic waves by randomly positioned grains, including coherent backscattering effects, quantitatively correctly explains many results of controlled laboratory experiments (e.g., Frisch 1968; Tsang, Kong, & Shin 1985; Akkermans et al. 1988; van der Mark et al. 1988; MacKintosh & John 1988; Barabanenkov et al. 1991; Mishchenko 1991c). According to this theory (e.g., Barabanenkov 1975; Prishivalko, Babenko, & Kuz'min 1984; Tsang, Ding, & Wen 1990), the diffusion contribution can be found by solving Chandrasekhar's (1960) vector radiative transfer equation (for reviews of the vector radiative transfer theory, see, e.g., Hansen & Travis 1974; Hovenier & van der Mee 1983; Ishimaru & Yeh 1984). At present, numerical calculations are possible for spherical (e.g., Hansen 1971; de Haan, Bosma, & Hovenier 1987) as well as for randomly oriented nonspherical (Mishchenko 1991a, b; Wauben & Hovenier 1992) regolithic grains. On the other hand, calculation of the coherent component $\boldsymbol{I}^C$ is a much more complicated problem. It is rather easy to calculate the coherent intensity I^C in the scalar approximation (e.g., van der Mark et al. 1988; Akkermans et al. 1988; Ishimaru & Tsang 1988; Ozrin 1992a). However, although the scalar approximation may be used for calculating coherent backscattering in the case of parallel incident and detected polarizations, it fails in calculations of the backscattered intensity for unpolarized incident light (Mishchenko & Dlugach 1992b; Mishchenko 1992a) and cannot be used for calculating the angular profile of the backscattered polarization. In this latter case, a rigorous vector theory of coherent backscattering must be used.

Unfortunately, this rigorous vector theory is still to be developed for grains of arbitrary size and refractive index. However, in calculations for grains much smaller than the wavelength, one may use the exact vector solution for coherent backscattering by Rayleigh scatterers found recently by Ozrin (1992b). Ozrin considered a semi-infinite random medium composed of pointlike nonabsorbing grains and, for the case of normal incidence of linearly polarized light, has found the angular distribution of the backscattered intensity for arbitrary scanning plane and arbitrary direction of the detected polarization. (Note that Ozrin assumed that the diffuse background given by the component $\boldsymbol{I}^D$ is phase-angle–independent. Therefore, his equations should be used with caution at phase angles greater than several degrees.) Ozrin's solution can easily be reformulated for the case of unpolarized incident light, and the angular profiles of the intensity I and the Stokes parameter Q near the backscattering direction can be calculated (due to the symmetry, the Stokes parameters U and V of the reflected light are identically equal to zero for the case of normal incidence of unpolarized light).

Specifically, assuming the perpendicularly incident, linearly polarized beam of unit intensity, Ozrin (1992b) has derived the following formula for the detected backscattered signal:

$$J(q, \varphi, \varphi_0) = J^D(\varphi, \varphi_0) + J^C(q, \varphi, \varphi_0) , \tag{2}$$

where the diffuse and coherent components are given, respectively, by

$$J^D(\varphi, \varphi_0) = \frac{3}{16\pi} \cos^2 \phi + \frac{3}{8\pi} [\cos^2 \phi F_{xx;xx}(0) + \sin^2 \phi F_{xx;yy}(0)] , \tag{3}$$

$$\begin{aligned} J^C(q, \varphi, \varphi_0) = \frac{3}{8\pi} \{&\cos^2 \varphi \cos^2 \varphi_0 F_{xx;xx}(q) + \sin^2 \varphi \sin^2 \varphi_0 F_{yy;yy}(q) + [\cos^2 \varphi \sin^2 \varphi_0 + \sin^2 \varphi \cos^2 \varphi_0] F_{xy;yx}(q) \\ &+ 2 \cos \varphi \cos \varphi_0 \sin \varphi \sin \varphi_0 [F_{xy;xy}(q) + F_{xx;yy}(q)]\} . \end{aligned} \tag{4}$$

Here, the angular parameter q is given by $q = kl\alpha$, l is the scattering mean free path given by $l = [nC_{sca}]^{-1}$, n is the number density of the grains, and C_{sca} is their scattering cross section, φ and φ_0 are the angles between the detected and incident polarizations and the scanning plane (i.e., plane through the vectors $\boldsymbol{n}_{ill}$ and $\boldsymbol{n}_{obs}$), respectively, $\phi = \varphi - \varphi_0$ is the angle between the detected and incident polarizations, and $F_{ij;lm}$ are some angular functions. For these functions, Ozrin has obtained the following simple semi-analytical expressions valid (within 2% accuracy) in the interval $0 \le q < 2$:

$$F_{xy;xy}(q) + \frac{1}{2} \cong \frac{0.85}{(0.99q^2 + 1)^{1/8}} , \tag{5}$$

$$F_{xy;yx}(q) \cong \frac{0.125}{0.57q^2 + 1} , \tag{6}$$

$$F_{xx;yy}(q) \cong \frac{1.07}{(1 + 1.26q)^{2.3}} , \tag{7}$$

$$F_{yy;yy}(q) - F_{xx;yy}(q) + \frac{1}{2} \cong \frac{0.975}{(8q^2 + 1)^{0.1}} , \tag{8}$$

$$F_{xx;xx}(q) - F_{yy;yy}(q) \cong \frac{0.95q^2}{1 + 5q^2} . \tag{9}$$

It should be emphasized here that, due to the interference nature of coherent backscattering, the backscattered coherent signal depends on the phase angle α only through the angular parameter $q = kl\alpha$.

Unpolarized incident light of unit intensity can be represented as a mixture of two linearly polarized beams with mutually perpendicular polarizations (with $\varphi_0 = 0$ and $\pi/2$) and intensities equal to $\frac{1}{2}$ (Chandrasekhar 1960). Therefore, from the definition of the Stokes parameters (van de Hulst 1957), we have for the intensity I and Stokes parameter Q of the backscattered light

$$I(\alpha) \equiv I(q) = \tfrac{1}{2}[J(q, 0, 0) + J(q, 0, \pi/2) + J(q, \pi/2, 0) + J(q, \pi/2, \pi/2)] , \tag{10}$$

$$Q(\alpha) \equiv Q(q) = \tfrac{1}{2}[J(q, 0, 0) + J(q, 0, \pi/2) - J(q, \pi/2, 0) - J(q, \pi/2, \pi/2)] . \tag{11}$$

Now, by using equations (2)–(11), we can calculate the angular profiles of the backscattered intensity I and Stokes parameter Q. Results of our calculations are given in Figures 5 and 6. In Figure 5, we plot the photometric enhancement factor ζ versus the angular parameter q. The enhancement factor ζ describes the angular profile of the photometric opposition effect and is defined as the ratio of the total reflected intensity to the diffuse background intensity:

$$\zeta(q) = I(q)/I^D = [I^D + I^C(q)]/I^D . \tag{12}$$

Note that $\zeta(0) \approx 1.54$, in agreement with calculations of Mishchenko (1992a). In Figure 6, the degree of linear polarization $P(q) = -Q(q)/I(q)$ is plotted.

From Figures 5 and 6, it is obvious that for grains much smaller than the wavelength, the photometric opposition effect is accompanied by the polarization opposition effect, the halfwidth at half-maximum α_{HM} of both effects being nearly the same and being given by $q_{HM} = kl\alpha_{HM} \approx 0.56$, or

$$\alpha_{HM} \approx \frac{0.56}{kl} . \tag{13}$$

This is the main result of our calculations. Note that in Figures 5 and 6, the enhancement factor ζ and polarization P are plotted as functions of the angular parameter $q = kl\alpha$. Therefore, Figures 5 and 6 are valid for any scattering grains provided that their size is much smaller than the wavelength. If the wavelength of light and the size, refractive index, and number density of the grains are specified, then the scattering mean free path l can be calculated, and both the enhancement factor and polarization can be replotted as functions of the phase angle $\alpha = q/kl$.

In the range of large angular parameters, where approximations (5)–(9) fail, equation (4) for the coherent contribution J^C is replaced by the asymptotic formula (Ozrin 1992b)

$$J^C(q, \varphi, \varphi_0) \cong \frac{9}{64q}\left[\cos^2\varphi\cos^2\varphi_0 + \frac{3}{8}\sin^2\varphi\sin^2\varphi_0 + \cos\varphi\cos\varphi_0\sin\varphi\sin\varphi_0\right] . \tag{14}$$

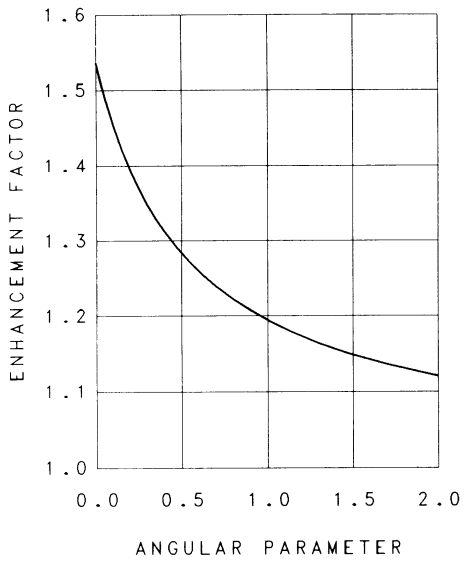

FIG. 5

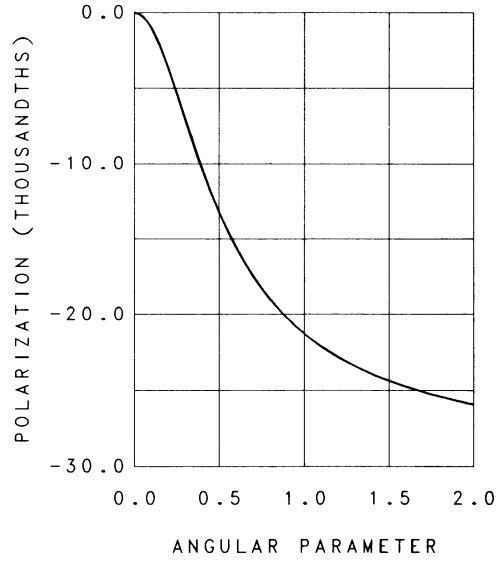

FIG. 6

FIG. 5.—Enhancement factor ζ vs. angular parameter q for a semi-infinite random medium composed of nonabsorbing, pointlike scatterers and illuminated by unpolarized, perpendicularly incident light.

FIG. 6.—Same as Fig. 5 for polarization P

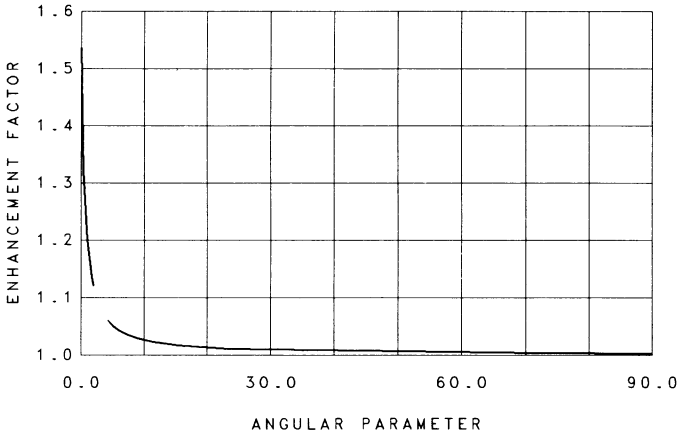

FIG. 7

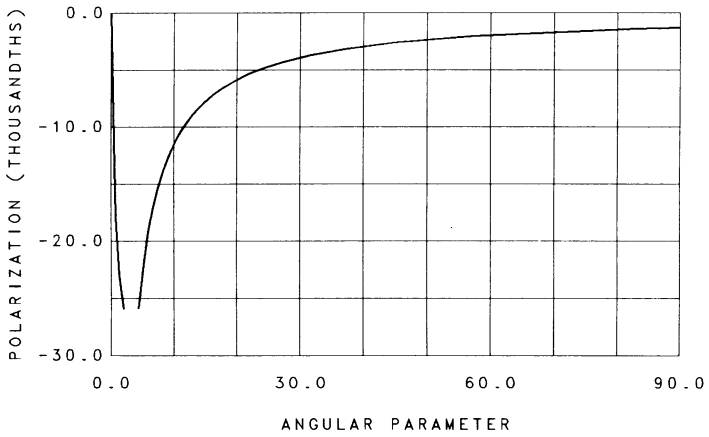

FIG. 8

FIG. 7.—Asymptotic behavior of the coherent photometric opposition effect
FIG. 8.—Asymptotic behavior of the coherent polarization opposition effect

In practice, this formula works for $q > 4$. The corresponding asymptotic behavior of the enhancement factor ζ and polarization P is shown in Figures 7 and 8, respectively. As follows from equation (14), at $q \gg 1$ both the enhancement factor and polarization are inversely proportional to the angular parameter. Therefore, the asymptotic curves in Figures 7 and 8 have typical hyperbolic shape. Note that equations (3) and (11) imply that, for unpolarized incident light, the diffuse component of the backscattered light is unpolarized for any angular parameters q. However, depending on the particular scattering problem, the diffuse component may be substantially polarized even at small angular parameters. Therefore, in such cases the coherent polarization shown in Figure 8 will be superposed on the diffuse, background polarization (see below).

The polarization opposition effect accompanying the photometric opposition effect was observed in controlled laboratory experiments by van Albada et al. (1988), although these authors exploited different terminology. Specifically, they used a random medium composed of spherical latex particles in water, illuminated that medium by a linearly polarized laser beam which was incident perpendicularly to the boundary of the medium, and measured the intensity of the reflected light for the copolarized and cross-polarized components. Measurements were performed in two scanning planes, the first of which was parallel (hereafter, subscript $\|$) and the second one was perpendicular (hereafter, subscript $\perp$) to the incident polarization. Due to coherent backscattering, van Albada et al. detected backscattering peaks in the intensity profiles for both the copolarized and cross-polarized components. They found that near the opposition, the cross-polarized intensity was the same for both scanning planes (i.e., $I_{\perp,\mathrm{crosspolar}} = I_{\|,\mathrm{crosspolar}}$). At the same time, the intensity profile for the copolarized component was spatially anisotropic for sub-wavelength particles. Specifically, while in exactly the opposition $I_{\perp,\mathrm{copolar}}(0)$ was equal to $I_{\|,\mathrm{copolar}}(0)$, at a small phase angle roughly equal to the angular semi-width of the opposition peaks the component $I_{\|,\mathrm{copolar}}$ became appreciably greater than the component $I_{\perp,\mathrm{copolar}}$. Obviously, in the case of unpolarized incident light this would result in the polarization opposition effect (Kolokolova et al. 1993).

van Albada et al. (see also van der Mark 1990) have given a clear qualitative explanation of the spatial anisotropy observed in their experiments. According to their explanation, the effect is due to the lowest-order scattering events. These lowest-order scattering events are significant for Rayleigh grains, which are strong side-scatterers and polarizers, and are not significant for large particles, for which singly scattered light is almost completely confined to a narrow cone in the forward direction and which are weak polarizers at most of scattering angles (Hansen & Travis 1974). Therefore, the spatial anisotropy must decrease with increasing grain size and disappear as scattering particles become comparable to or larger than the wavelength. Indeed, in accordance with this conclusion, van Albada et al. did not found the spatial anisotropy in their measurements of the coherent copolarized intensity peak for latex particles larger than the wavelength (see also Hapke et al. 1991).

Thus, it follows from our theoretical calculations and the work by Albada et al. that (1) the polarization opposition effect is produced by sub-wavelength grains, (2) its amplitude decreases with increasing grain size and disappears as grains become comparable to or larger than the wavelength, and (3) if produced, the polarization opposition effect has the same angular semi-width as the photometric opposition effect. Unlike the polarization opposition effect, the photometric opposition effect can be produced by grains of practically any size, although its angular width and (to a lesser degree) amplitude will, of course, depend on the grain characteristics.

Equation (13) shows that the angular semi-width of the coherent backscattering effects is inversely proportional to the product kl. As was noted above, this relationship is a direct consequence of the interference nature of coherent backscattering. Moreover, as follows from the theory of coherent backscattering (e.g., Akkermans et al. 1988), the same relationship is valid for finite-sized, anisotropically scattering grains provided that the scattering mean free path l is replaced by the transport mean free path l_{tr} given by (e.g., Ishimaru 1978)

$$l_{\mathrm{tr}} = \frac{1}{nC_{\mathrm{sca}}(1 - \langle \cos\theta \rangle)}, \tag{15}$$

where $\langle \cos\theta \rangle$ is the mean cosine of the scattering angle (for pointlike scatterers, $\langle \cos\theta \rangle = 0$ and $l_{\mathrm{tr}} = l$). However, earlier the proportionality factor $q_{\mathrm{HM}} = kl_{\mathrm{tr}}\alpha_{\mathrm{HM}}$ was measured and calculated only for the cases of linearly or circularly polarized incident and

detected light (e.g., Etemad et al. 1987; Wolf et al. 1988). Therefore, this factor depended on whether the detected polarization was parallel or perpendicular to the incident polarization and on whether the incident polarization was parallel or perpendicular to the scanning plane. Our calculations based on the Ozrin vector theory show for the first time that for the practically important case of unpolarized incident light, the factor q_{HM} is close to 0.56.

To calculate theoretically the angular semi-width of the coherent opposition effects, the transport mean free path must first be computed. To compute l_{tr} for densely packed grains, we use a dense-medium light-scattering theory based on introducing the so-called static structure factor (e.g., Wolf et al. 1988; Mishchenko 1992b). As is shown by Wolf et al. (1988), this theory is in good agreement with the results of their controlled laboratory experiments. As an example, in Figure 9 calculations are reported for spherical grains with the index of refraction $N = 1.31$, corresponding to water ice at visible wavelengths, and different values of the filling factor f (i.e., the fraction of a volume occupied by the grains). The scatter of grain radii is modeled by the standard gamma distribution (Hansen & Hovenier 1974)

$$n(r) \propto r^{(1-3b)/b} \exp\left(-\frac{r}{ab}\right), \tag{16}$$

where a is the effective radius and b is the effective variance. In Figure 9, α_{HM} is plotted versus a dimensionless size parameter $y = a/\lambda$ for two values of the effective variance b. The first of these values $b = 0.05$ corresponds to a narrow size distribution, while the distribution with $b = 0.15$ is moderately broad.

Note that equation (13) is relevant to the case of normal incidence of light on the surface. As was shown by Gorodnichev, Dudarev, & Rogozkin (1989, 1990), in the case of oblique incidence α_{HM} is inversely proportional to the cosine of the angle of incidence ϑ measured from the inward normal to the surface:

$$\alpha_{HM} \propto 1/\cos\vartheta\ . \tag{17}$$

Therefore, for macroscopically rough surfaces the angular semi-width of the opposition effects will be somewhat larger than that calculated from equation (13). In the first approximation, this enlargement is given by the factor $\langle 1/\cos\vartheta_0\rangle$, where ϑ_0 is the local surface slope, and angle brackets denote the ensemble average.

Apparently, the polarization opposition effect was observed for the first time in laboratory polarimetric measurements by Lyot (1929), although he did not measure simultaneously the intensity of the scattered light and, therefore, did not detect the accompanying photometric opposition effect. Figure 10 shows his measurements for a magnesia sample obtained by burning a tape of magnesium under a glass plate until the deposit on the plate was completely opaque. Lyot's measurements seem to be very interesting since they demonstrate the full angular profile of the polarization opposition effect including the sharp rise of negative polarization at almost zero phase angles and asymptotic behavior at phase angles much greater than α_{HM}. Lyot describes the

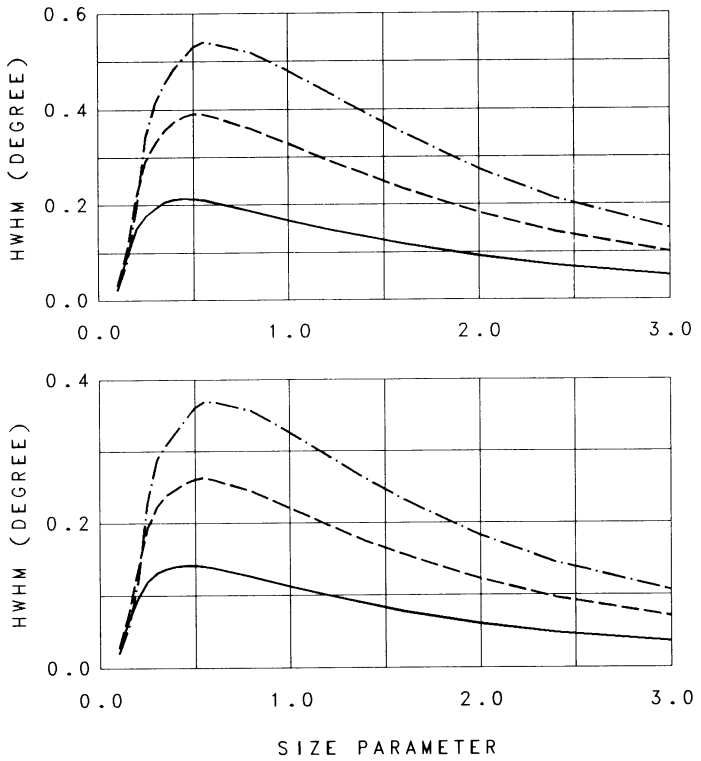

FIG. 9.—Half-width at half-maximum of the coherent opposition effects α_{HM} vs. a dimensionless size parameter $y = a/\lambda$ for the refractive index $N = 1.31$, effective variance $b = 0.05$ (*upper panel*) and 0.15 (*lower panel*), and three values of the filling factor $f = 0.1$ (*solid lines*), 0.2 (*dashed lines*), and 0.3 (*dot-dashed lines*).

measured polarization phase curve as "puzzling" and attributes it to the size of the magnesia grains which was very small. Unfortunately, Lyot does not give an estimate of the grain size. Apparently, the grains were not small enough to produce as large amplitude of the polarization opposition effect as that calculated theoretically for pointlike scatterers (cf. Figs. 8 and 10). However, the angular shape of the measured and theoretically calculated phase curves is exactly the same up to $\alpha \approx 16°$, as is shown in Figure 10. At larger phase angles, the background polarization becomes increasingly positive, and the resulting polarization changes sign.

Geake & Geake (1990) have published an extensive set of laboratory polarimetric measurements of light scattering by powders of alumina (Al_2O_3) grains. By changing both the mean grain radius a and wavelength λ, they varied the size parameter $y = a/\lambda$ from 0.0465 to 37.5. Their measurements for the smallest grains (crystals) evidently demonstrate the polarization opposition effect like that shown in Figures 8 and 10, which disappears as grains become larger than the wavelength. For the largest grains, Geake and Geake measured a smooth, size-parameter–independent negative polarization branch which, apparently, is produced by the Wolff mechanism (Wolff 1975). The absence of the general vector theory of coherent backscattering for grains of arbitrary size does not enable us to reproduce theoretically the measured amplitude of the polarization opposition effect. However, the measurements by Geake and Geake can be used to verify the theoretical relationship given by equation (13). Although, instead of α_{HM}, Geake and Geake measured the phase angle α_{min} at which polarization reaches its minimum (i.e., maximum negative) value, it follows from their polarization phase curves that the quantity $\alpha_{min}/4$ is a good estimate for the angular semiwidth α_{HM} (cf. also Figs. 2, 6, and 10). Unfortunately, when varying the mean grain size, Geake and Geake did not measure the porosity of their samples. However, the measurements for the same 0.3 μm sample were made at four different wavelengths, which gives four values of the size parameter y for constant filling factor f, refractive index N, and effective variance of the grain size distribution b. The refractive index of alumina is known ($N \approx 1.77$). Therefore, it seemed possible to fit the measured angular semi-width of the polarization opposition effect theoretically by varying the unknown parameters f and b. Indeed, our calculations have shown that a reasonably good fit to the measurements can be obtained for $b \simeq 0.2$ and $f \simeq 0.2$ (Fig. 11). Note that Geake and Geake describe the size distribution of the scattering grains as very narrow. Therefore, the effective variance $b \simeq 0.2$ may be the consequence of using broad filters (and thus nonmonocromatic light) rather than an actual characteristic of the grain size distribution.

It follows from the measurements by Geake and Geake that, apparently, several quite different physical mechanisms can produce negative polarization at small phase angles. Small grains produce the sharp polarization opposition effect via the coherent backscattering mechanism, while large grains and/or macroscopic surface irregularities can produce a smooth negative polarization branch via the Wolff mechanism (Wolff 1975). Of course, depending on the size and refractive index of the grains, negative polarization at small phase angles can also be produced by ordinary Mie scattering (Hansen & Travis 1974).

Finally we note that in laboratory measurements by Oetking (1966), bidirectional reflectivity of several high albedo samples was measured. Although the minimum phase angle in Oetking's measurements was relatively large (1°), his measurements for a heavily smoked MgO surface and fine Al_2O_3 powders definitely show a sharp opposition surge with angular semi-width of a degree or even less. With increasing size of alumina grains, the amplitude of the opposition effect measured at $\alpha = 1°$ decreases, which, apparently, means that the opposition surge becomes narrower and almost unobservable with the apparatus used (cf. Mishchenko 1992b). For the MgO sample, the angular width of the opposition effect increases with increasing angle of incidence, which is in qualitative agreement with equation (17). Thus, Oetking was, apparently, the first to observe the coherent photometric opposition effect, and his measurements for the magnesia and alumina samples may, in a sense, be considered a photometric supplement to the polarimetric measurements by Lyot and Geake and Geake.

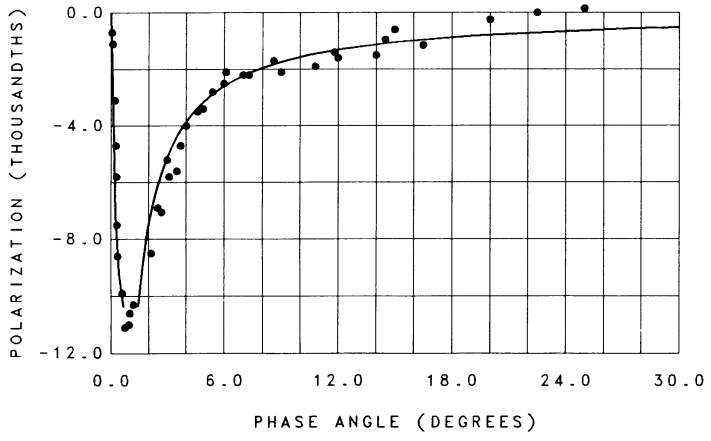

FIG. 10

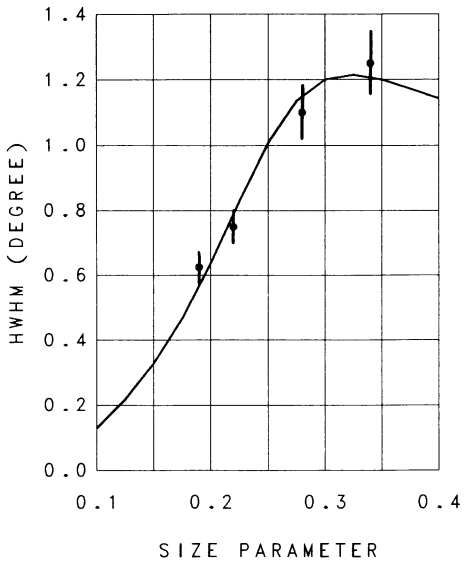

FIG. 11

FIG. 10.—Laboratory polarimetric measurements for a magnesia sample (Lyot 1929). The solid curve is obtained from that shown in Figure 8 by assuming $kl = 3$ (i.e., $\alpha = q/3$) and reducing the computed polarization by a factor of 2.5.

FIG. 11.—Same as Fig. 9 for $N = 1.77$, $b = 0.21$, and $f = 0.205$. Filled circles show measurements by Geake and Geake (1990) for 0.3 μm alumina grains at four wavelengths.

3. ANALYSIS OF OBSERVATIONS OF SATURN'S RINGS

As was pointed out above, in this paper we assume that Saturn's rings are a dense monolayer of macroscopic bodies. Therefore, mutual shadowing among these bodies may be neglected or results in an intensity peak that is much wider than the observed spike with semi-width of a few tenths of a degree and thus is practically indistinguishable from the smooth component of the photometric phase curve. Also we assume that macroscopic ring particles are partially covered with a layer of submicrometer-sized regolithic ice grains which, via coherent backscattering of sunlight, gives rise to the photometric opposition effect observed in the visible (Mishchenko & Dlugach 1992a).

The polarization phase curve observed for Saturn's rings (Lyot 1929; Dollfus 1979; Johnson et al. 1980) has the following spectral features. (1) In the visible, sharp rise of negative polarization is observed at phase angles less than a degree (Figs. 2 and 3). The angular semi-width of this feature is roughly equal to that of the photometric opposition effect, which is characteristic for the coherent polarization opposition effect. However, at larger phase angles the shape of the polarization phase curve differs from that measured and calculated for the pure coherent polarization opposition effect (cf. Figs. 2, 3, 8, and 10). (2) In the near ultraviolet, no signs of the sharp rise of negative polarization are seen, and the observed polarization has a smooth, nearly parabolic negative branch (Fig. 12). As follows from our discussion, this spectral behavior can be explained by suggesting that in the visible, the grains that produce the photometric opposition effect are small enough to produce also the polarization opposition effect, which is superposed on a nearly wavelength-independent, parabolic negative polarization branch of unknown origin. In the near ultraviolet, the grains become comparable to or greater than the wavelength, the polarization opposition effect disappears, and we observe the negative polarization branch itself.

Our calculations shown in Figure 9 demonstrate that to produce the observed α_{HM} of about 0°.3 in the visible, the regolithic ice grains should have radii of about several tenths of micrometer. As follows from the measurements of Franklin & Cook (1965), the angular semi-width of the photometric opposition effect is practically the same in the B (448 nm) and V (554 nm) filters (Fig. 1). Therefore, it is reasonable to suggest that the size parameter $y = a/\lambda$ for the regolithic ice grains is close to 0.5 (where the derivative $d\alpha_{HM}/dy$ is close to zero [Fig. 9]), and thus the grain effective radius is of about 0.3 μm. Unfortunately, the absence of the relevant vector theory of weak localization for particles of arbitrary size does not enable us to use the polarimetric observational data for determining the size of the regolithic ice grains more accurately and, of course, makes our explanation of the polarization opposition effect indicative rather than definitive. Obviously, the grains cannot be much smaller than roughly 0.5 μm. Indeed, in the visible, they do not produce as strong polarization opposition effect as that calculated theoretically for pointlike scatterers (compare Figs. 2, 3, and 6). Also, at 350 nm, the polarization opposition effect seems to be absent at all (Fig. 12). Since the refractive index of latex in water (1.2) is close to the index of refraction of water ice (1.31), it seems worthwhile to note that van Albada et al. (1988) observed the spatial anisotropy (and thus the polarization opposition effect) for latex particles with $y \approx 0.23$ and did not find this effect for particles with $y \approx 1.1$. Thus, the polarization opposition effect for scattering particles with small refractive indices should disappear somewhere in the range of particle size parameters $0.23 < y < 1.1$, which is in agreement with our estimate of the effective grain radius of about 0.3 μm.

Note that the presence of submicrometer-sized ice grains in the ring system also follows from the explanation of the famous radial "spokes" (e.g., Doyle & Grün 1990). The possible origin of these grains is discussed by Smoluchowski (1983). It may be noted that small ice grains seem to be widespread throughout the outer solar system, in accord with the analysis of Clark, Fanale, & Zent (1983). In particular, they form the E ring of Saturn (Pang et al. 1984; Showalter, Cuzzi, & Larson 1991), and, apparently, produce the unusually narrow opposition effect observed for Europa and icy Uranian satellites (Mishchenko 1992b).

It may well be that only a part of the surface of ring bodies is covered with the 0.3 μm grains. The rest of the surface, which, most

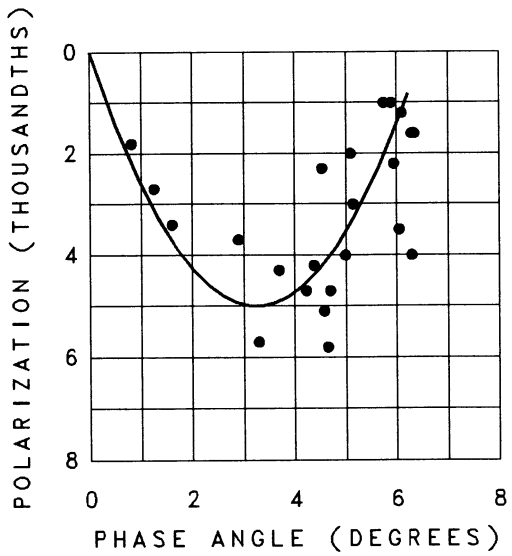

FIG. 12.—Polarization phase curve for the B ring of Saturn at 350 nm (Dollfus 1979)

likely, is covered with much larger grains, cannot contribute to the observed photometric opposition effect with angular semi-width of about 0°.3 (see Fig. 9) and does not produce the polarization opposition effect. However, this latter part of the surface contributes to the incoherent, background radiation and thus reduces the observed amplitudes of the coherent opposition effects. One more incoherent contribution to the background radiation comes from the light multiply reflected by different surface elements, these multiple reflections being due to macroscopic surface roughness of the ring bodies with scale much greater than the mean grain size and to successive reflections by different ring bodies. These two additional incoherent contributions, which raise the background intensity, can explain qualitatively why the observed amplitude of the photometric opposition effect is smaller than that calculated theoretically for submicrometer-sized grains (Mishchenko & Dlugach 1992a). Also, they can partly explain why the measured amplitude of the polarization opposition effect (Figs. 2 and 3) is smaller than that calculated theoretically for pointlike scatterers (Fig. 6) (as was pointed out earlier, an additional explanation of this fact is that the regolithic grains producing the polarization opposition effect are not small enough to be pure Rayleigh scatterers). However, it is very difficult to obtain accurate quantitative estimates of their influence on the amplitudes of the photometric and polarization opposition effects, because this will require detailed information about the spatial distribution of ring bodies and morphology and composition of the upper, optically active regolithic layer which may be very nonuniform over the surface. In other words, the observed amplitudes of the photometric and polarization opposition effects depend not only on the physical properties of the grains that produce these effects, but also on the ring structure and surface morphology and composition on the whole. In addition, to accurately reproduce the observed photometric and polarization phase curves, one must be able to calculate theoretically (1) light scattering by a macroscopically rough surface covered with transparent, densely packed grains much greater than the wavelength and (2) multiple light reflections by densely distributed ring bodies. Unfortunately, at present there are no relevant physical theories that would enable such calculations. On the other hand, the angular semi-width of the coherent opposition effects α_{HM} is not influenced by the two above-mentioned incoherent contributions at all. Therefore, this characteristic contains more reliable and retrievable information about the grains that produce the opposition effects.

It follows from our analysis that coherent backscattering alone cannot explain the presence of the negative polarization branch on the polarization phase curve of Saturn's A and B rings. Indeed, it appears that the polarization opposition effect is present in the visible and is simply superposed on the negative polarization branch. At shorter wavelengths, the polarization opposition effect seems to disappear, and we observe the negative polarization branch itself.

Negative polarization at small phase angles has been observed for many atmosphereless bodies, and its origin is still not clear enough. Recently, Shkuratov (1989) and Muinonen (1990) have suggested that the coherent backscattering mechanism might be the universal explanation of negative polarization. However, as was noted above, coherent backscattering alone does not explain negative polarization measured for high albedo laboratory samples by Geake & Geake (1990) and observed for Saturn's rings. Apparently, the origin of the negative polarization branch may be different for surfaces of different texture and covered with different materials.

Finally we note that a remarkable opposition brightening similar to that for Saturn's rings has also been observed for icy Uranian satellites (Brown & Cruikshank 1983; Goguen et al. 1989), Europa (Domingue et al. 1991; Thompson & Lockwood 1992), and high albedo E-type asteroids 44 Nysa and 64 Angelina (Harris et al. 1989; Lagerkvist et al. 1992). It follows from our analysis that if the observed photometric opposition effect is produced by coherent backscattering, and the grains responsible for the opposition brightening are smaller than the wavelength, then the polarization opposition effect should also be observed for these objects at phase angles less than 1 degree.

The author is indebted to an anonymous reviewer for valuable comments and suggestions, E. G. Yanovitskij, L. O. Kolokolova, Yu. G. Shkuratov, R. Smoluchowski, and B. Cairns for useful discussions, and J. E. Geake for pointing out that Figure 5 in Geake & Geake (1990) could be explained in terms of coherent backscattering. He gratefully acknowledges programming support from A. Wolf and A. Walker and thanks Z. Wai, L. Del Valle, and J. L. Mendoza for technical assistance.

REFERENCES

Akkermans, P. E., Wolf, P. E., Maynard, R., & Maret, G. 1988, J. Phys. (Paris), 49, 77
Barabanenkov, Yu. N. 1975, Soviet Phys.–Uspekhi, 18, 673
Barabanenkov, Yu. N., Kratsov, Yu. A., Ozrin, V. D., & Saichev, A. I. 1991, in Progress in Optics XXIX, ed. E. Wolf (Amsterdam: North-Holland), 65
Bobrov, M. S. 1961, AZh, 38, 669
Bowell, E., Hapke, B., Domingue, D., Lumme, K., Peltoniemi, J., & Harris, A. W. 1989, in Asteroids II, ed. R. P. Binzel, T. Gehrels, & M. S. Matthews (Tucson: Univ. Arizona Press), 524
Bridges, F. G., Hatzes, A., & Lin, D. N. C. 1984, Nature, 309, 333
Brown, R. H., & Cruikshank, D. P. 1983, Icarus, 55, 83
Chandrasekhar, S. 1960, Radiative Transfer (NY: Dover)
Clark, R. N., Fanale, F. P., & Zent, A. P. 1983, Icarus, 56, 233
Cook, A. F., Franklin, F. A., & Palluconi, F. D. 1973, Icarus, 18, 317
de Haan, J. F., Bosma, P. B., & Hovenier, J. W. 1987, A&A, 183, 371
Dollfus, A. 1979, Icarus, 37, 404
Dollfus, A., Wolff, M., Geake, J. E., Lupishko, D. F., & Dougherty, L. M. 1989, in Asteroids II, ed. R. P. Binzel, T. Gehrels, & M. S. Matthews (Tucson: Univ. Arizona Press), 594
Domingue, D. L., Hapke, B. W., Lockwood, G. W., & Thompson, D. T. 1991, Icarus, 90, 30
Doyle, L. R., & Grün, E. 1990, Icarus, 85, 168
Etemad, S., Thompson, R., Andrejco, M. J., John, S., & MacKintosh, F. C. 1987, Phys. Rev. Lett., 59, 1420
Franklin, F. A., & Cook, A. F. 1965, AJ, 70, 704
———. 1974, Icarus, 23, 355
Frisch, U. 1968, in Probabilistic Methods in Applied Mathematics, ed. A. T. Bharucha-Reid (NY: Academic Press), 75
Geake, J. E., & Dollfus, A. 1986, MNRAS, 218, 75
Geake, J. E., & Geake, M. 1990, MNRAS, 245, 46
Goguen, J. D., Hammel, H. B., & Brown, R. H. 1989, Icarus, 77, 239
Gorodnichev, E. E., Dudarev, S. L., & Rogozkin, D. B. 1989, Zh. Eksper. Teor. Fiz., 96, 847
———. 1990, Phys. Lett. A, 144, 48
Hansen, J. E. 1971, J. Atmos. Sci., 28, 1400
Hansen, J. E., & Hovenier, J. W. 1974, J. Atmos. Sci., 31, 1137
Hansen, J. E., & Travis, L. D. 1974, Space Sci. Rev., 16, 527
Hapke, B. 1986, Icarus, 67, 264
Hapke, B. W., Nelson, R. M., Smythe, W. D., Gharakanian, V., Horn, L. J., & Lane, A. L. 1991, BAAS, 23, 1139
Harris, A. W., et al. 1989, Icarus, 81, 365
Hovenier, J. W., & van der Mee, C. V. M. 1983, A&A, 128, 1
Irvine, W. M. 1966, J. Geophys. Res., 71, 2931
Ishimaru, A. 1978, Wave Propagation and Scattering in Random Media, Vol. 1, Single Scattering and Transport Theory (NY: Academic Press)
Ishimaru, A., & Tsang, L. 1988, J. Opt. Soc. Am. A, 5, 228
Ishimaru, A., & Yeh, C. W. 1984, J. Opt. Soc. Am. A, 1, 359
Johnson, P. E., Kemp, J. C., King, R., & Barbour, M. S. 1980, Nature, 283, 146

Kolokolova, L. O. 1990, Icarus, 84, 305
Kolokolova, L. O., Mishchenko, M. I., & Wolff, M. 1993, MNRAS, 260, 550
Kuga, Y., & Ishimaru, A. 1984, J. Opt. Soc. Am. A, 1, 831
Lagerkvist, C.-I., Magnusson, P., Williams, I. P., Buontempo, M. E., Argyle, R. W., & Morrison, L. V. 1992, A&AS, 94, 43
Lumme, K., & Bowell, E. 1981, AJ, 86, 1694
Lumme, K., Irvine, W. M., & Esposito, L. W. 1983, Icarus, 53, 174
Lyot, B. 1929, Ann. Obs. Paris 8, No. 1; English transl. NASA TT F-187 (1964)
MacKintosh, F. C., & John, S. 1988, Phys. Rev., B 37, 1884
Mishchenko, M. I. 1991a, J. Opt. Soc. Am. A, 8, 871
———. 1991b, J. Quant. Spectros. Rad. Transf., 46, 171
———. 1991c, Phys. Rev. B, 44, 12597
———. 1992a, J. Opt. Soc. Am. A, 9, 978
———. 1992b, Ap&SS, 194, 327
Mishchenko, M. I., & Dlugach, J. M. 1992a, MNRAS, 254, 15P
———. 1992b, Ap&SS, 189, 151
Morozhenko, A. V., & Yanovitskij, E. G. 1971, AZh., 48, 172
Muinonen, K. 1990, Ph.D. thesis, Univ. Helsinki
Müller, G. 1893, Potsdam Pub. 8
Oetking, P. 1966, J. Geophys. Res., 71, 2505
Ozrin, V. D. 1992a, Phys. Lett. A, 162, 341
———. 1992b, Waves Random Med., 2, 141
Pang, K. D., Voge, C., Rhoads, J. W., & Ajello, J. M. 1984, G. Geophys. Res., 89, 9459
Prishivalko, A. P., Babenko, V. A., & Kuz'min, V. N. 1984, Scattering and Absorption of Light by Inhomogeneous and Anisotropic Particles (Minsk: Nauka i Tekhnika)
Shkuratov, Yu. G. 1989, Sol. Syst. Res., 23, 111
Showalter, M. R., Cuzzi, J. N., & Larson, S. M. 1991, Icarus, 94, 451
Smoluchowski, R. 1983, Icarus, 54, 263
Thompson, D. T., & Lockwood, G. W. 1992, J. Geophys. Res., 97, 14761
Tsang, L., Ding, K. H., & Wen, B. 1990, in Progress in Electromagnetic Research 3, ed. J. A. Kong (NY: Elsevier), 75
Tsang, L., Kong, J. A., & Shin, R. T. 1985, Theory of Microwave Remote Sensing (NY: Wiley-Interscience)
van Albada, M. P., van der Mark, M. B., & Lagendijk, A. 1988, J. Phys. D, 21, S28
van de Hulst, H. C. 1957, Light Scattering by Small Particles (NY: Wiley)
van der Mark, M. B. 1990, Ph.D. thesis, Amsterdam Univ.
van der Mark, M. B., van Albada, M. P., & Lagendijk, A. 1988, Phys. Rev. B, 37, 3575
von Seeliger, H. 1887, Abhandl. Bayer. Akad. Wiss. Kl. II, 16, 405
Wauben, W. M. F., & Hovenier, J. W. 1992, J. Quant. Spectros. Rad. Transf., 47, 491
Wisdom, J., & Tremaine, S. 1988, AJ, 95, 925
Wolf, P. E., Maret, G., Akkermans, E., & Maynard, R. 1988, J. Phys. (Paris), 49, 63
Wolff, M. 1975, Appl. Opt., 14, 1395
———. 1980, Icarus, 44, 780
Wolff, M., & Dollfus, A. 1990, Appl. Opt., 29, 1496